UNIVERSITÀ DI PARMA
ARCHIVIO DELLA RICERCA

University of Parma Research Repository

Processing and characterization of novel borophosphate glasses and fibers for medical applications

note finali coverpage

(Article begins on next page)

26 July 2025

Processing and characterization of novel borophosphate glasses and fibers for medical applications

Jonathan Massera[1,2,*], Yaroslav Shpotyuk[3], Fantine Sabatier[4], Thierry Jouan[3], Catherine Boussard-Plédel[3], Claire Roiland[3], Bruno Bureau[3], Laeticia Petit[4,5], Nadia G. Boetti[6], Daniel Milanese[6], Leena Hupa[4]

[1]Tampere University of Technology, Department of Electronics and Communications Engineering, Korkeakoulunkatu 3, FI-33720 Tampere, Finland
[2]BioMediTech, Tampere, Finland
[3]Equipe Verres et Céramiques, UMR-CNRS 6226, Sciences Chimiques de Rennes, Université de Rennes I, F-35042 Rennes Cedex, France
[4]Johan Gadolin Process Chemistry Centre, Åbo Akademi University, Biskopsgatan 8, FI-20500 Turku, Finland
[5]nLIGHT Corporation, Sorronrinne 9, FI-08500 Lohja, Finland
[6]Politecnico di Torino, DISAT, Istituto di Ingegneria e Fisica dei Materiali, Corso Duca degli Abruzzi 24, I-10129 Torino, Italy
* Corresponding author at: Tampere University of Technology, Department of Electronics and Communications Engineering, Korkeakoulunkatu 3, FI-33720 Tampere, Finland. E-mail address: jonathan.massera@tut.fi (J. Massera).

Abstract

In this paper, we investigate the effect of P_2O_5 substitution by B_2O_3 in the $(50 - x)P_2O_5 \cdot 20CaO \cdot 20SrO \cdot 10Na_2O \cdot x\,B_2O_3$ glass system (x from 0 to 5 mol%) on the thermal and structural properties and also on the glass reactivity in simulated body fluid. The goal is to develop new glass candidates for biomedical glass fibers. The addition of B_2O_3 at the expense of P_2O_5 increases the refractive index of the glass and also the thermal stability of the glass indicating that these glasses are promising glasses for fiber drawing. Thus, within such glass composition, the core of a core–clad fiber has a larger concentration of B_2O_3 than the clad of the fiber to enable the light to propagate inside the core. All the investigated glasses form a calcium phosphate layer at their surface when immersed in simulated body fluid. It was found that small addition of B_2O_3 (1.25 mol%) leads to a decrease in the initial dissolution rate and a delayed layer formation. However, with increasing B_2O_3 content, the chemical durability decreased slightly but was higher than for the B-free glass. In addition, formation of the calcium phosphate layer was further delayed. This suggests that small contents of B_2O_3 led to formation of P–O–B bonds and only few BO_4 units, increasing the chemical durability. At higher B_2O_3 contents, the amount of BO_4 units increases which makes the glass network slightly more prone to be hydrolyzed. Thus, formation of BO_4 units induced by the addition of B_2O_3 at the expense of P_2O_5 reduces the reactivity of the glass in SBF. Borophosphate fibers were successfully drawn from preform. As expected from the bioresponse of the bulk glasses in simulated body fluid, the reduction in the intensity of the light transmitted is less and slower in a borophosphate fiber than in a phosphate fiber upon immersion.

1. Introduction

Biomaterials are an integral and vital part of our modern health-care system. Hand in hand with more sophisticated solutions coming on the market, the demand on biomaterials based on biomedical glass fibers has increased in the past decade. Fibers based on bioactive glasses can be used for reinforcement in composite [1,2] or biosensing [3]. Due to their biocompatibility, the silica based glasses such as 45S5 [4] and S53P4 [5] are well-known candidates for different biomedical applications including bone-grafting. However, these glasses are prone to crystallize at temperatures typical for fiber drawing [6]. The problems with crystallization may, however, be solved by developing new bioactive glass compositions with thermal properties better suited for fiber drawing processes.

Phosphate glasses are good alternatives to silicate glasses in biomedical applications, such as in bone repair and reconstruction [7]. Recently, new types of bioresorbable borophosphate glasses were found to be good choices for fiber drawing due to their suitable forming proper- ties [8]. Borophosphate glass fibers are good candidates for soft tissue engineering applications involving muscles, ligaments, and tendons. In these, the tissue has, similarly to the glass fibers a high degree of anisotropy.

Borate glasses were found to accelerate the formation of a hydroxy- apatite layer and bond to bone [9]. The bioactivity of calcium phosphate glasses was favored by the addition of boron due to the ability of boron to change coordination and to attach hydroxyl groups at the surface of the glasses [10]. The incorporation of boron into the P_2O_5–CaO–Na_2O– MgO glass system showed favorable effects on the cell metabolic activity, proliferation, and morphology [11].

In our previous study, the effect of partial substitution of SrO for CaO on the thermal and bioactivity properties of phosphate glasses in the P_2O_5–CaO–SrO–Na_2O glass system was reported [12]. SrO containing glasses are of interest since traces of Sr are present in the human body [13].

Table 1
Thermal properties of the investigated glasses.

	Density (g/cm^3) ±0.02 g/cm^3	$T_g \pm 2$ °C	$T_x \pm 2$ °C	$\Delta T = T_x - T_g$ °C	Refractive index at ±0.001		
					633 nm	1061 nm	1312 nm
B0	2.80	444	587	143	1.538	1.530	1.527
B1.25	2.83	451	629	178	1.542	1.534	1.531
B2.5	2.85	451	662	211	1.545	1.536	1.533
B3.75	2.88	462	670	208	1.547	1.539	1.536
B5	2.90	465	672	205	1.549	1.541	1.538

Moreover, it has been shown that Sr can easily replace Ca in the mineral part of the bone to form a stronger bone [14]. In our previous study [12], we showed that SrO-containing phosphate glasses are promising glasses for fiber drawing from preforms. We also found that the addition of SrO at the expense of CaO restrains the leaching of phosphate ions while maintaining similar surface reactivity than the Sr-free phosphate glasses. Additionally, partial to full substitution of CaO for SrO has been found to enhance adhesion and proliferation of cells [15]. Howev- er, the composition of the reaction layer forming at the surface of these glasses is closer to dicalcium phosphate dihydrate (DCPD) than hydroxyapatite (HA) [12]. In order to reach Ca/P ratio closer to 1.6 and to increase the bioactivity of the phosphate-based glasses, new glasses were prepared by partially replacing P_2O_5 by B_2O_3.

In this work we study the effect of B_2O_3 addition on the thermal, structural and bioactive properties of phosphate glasses in the P_2O_5– CaO–SrO–Na_2O glass system. We also discuss the impact of the fiber drawing on those properties. Thermal properties of the glasses were measured using a differential thermal analyzer (DTA). Structural characterization of the studied glasses was performed using combination of experimental tools such as NMR, Raman and IR spectroscopies. The in-vitro testing was performed in simulated body fluid.

2. Experimental section

The glasses with the composition $(50 - x)P_2O_5 \cdot 20CaO \cdot 20SrO \cdot 10Na_2O \cdot x \ B_2O_3$ with x = 0, 1.25, 2.5, 3.75 and 5 (mol %) (labeled respectively B0, B1.25, B2.5, B3.75 and B5) were prepared using the standard melting method in a platinum crucible. $NaPO_3$, H_3BO_3, $SrCO_3$, $CaCO_3$ and $(NH_4)_2HPO_4$ were used as raw materials. $Sr(PO_3)_2$ and $Ca(PO_3)_2$ precursors were first independently prepared using a slow heating rate up to 900 °C. The precursors were mixed with the other raw materials and melted in the platinum crucible at 1200 °C. The melts were poured on a brass mold and the resulting glasses were annealed at 40 °C below their respective glass transition temperature for 4 h.

Unclad monoindex fibers were drawn by using the well-known "rod" method with a specially designed drawing tower. Before drawing, the system was purged with an Ar gas laminar flow at the rate of 3 L/min in order to lower the moisture concentration. The thermal gradient of the drawing furnace permits the softening of the preform just above its lower extremity. In order to ensure that the draw conditions do not induce either nucleation or crystallization, the temperature profiles of the draw furnace (hot zone and pre-heat zone) were precisely mapped and the dwell time in these zones was controlled prior to and during the drawing. A narrow (5 mm length) drawing furnace was used to decrease the time of presence of glass rod in the critical high- temperature zone. The preforms were drawn at 600 °C under a He gas laminar flow of 2.5 L/min to create an inert atmosphere around the preform. The fiber was then fixed on the drum in rotary motion. A computer system based on LabView software was used to control the fiber diameter and drawing tension. Fibers were drawn to a diameter of ~ 125 μm at a rate of 10.1 m/min with a feed rate at 2 mm/min. Nominally, 50 m of single core fiber was obtained for each drawing run. The uncoated fibers (without any protective polymer layer) were used for measurement of the thermal, structural and optical properties.

A Scanning Electron Microscope from Leo 1530 Gemini from Zeiss coupled with an Energy Dispersive X-Ray Analyzer (SEM/EDXA) from Vantage by Thermo Electron Corporation was used to analyze the oxide composition of the samples. The compositions of the as- prepared glasses were found to be in accordance with the theoretical ones, within the accuracy of measurement (~1.5 mol%).

The glass transition (T_g) and onset of crystallization (T_x) temperatures of the glasses were measured by Differential Thermal Analysis (DTA, Netszch F1 JUPITER) at a heating rate of 15 °C·min^{-1}. The T_g was taken at the inflection point of the endotherm, as obtained by taking the first derivative of the DSC curve. The T_x was measured at the onset of the exothermic peak. The characteristic temperatures were determined with an accuracy of ±2 °C.

The refractive index (RI) was measured at several wavelengths with a fully automated Metricon 2010 prism-coupler refractometer in order to determine the wavelength-dependent RI distribution curve. The accuracy of the measurement was estimated to ±0.001.

The IR absorption spectra of the glasses were recorded using a Perkin Elmer FTIR in Attenuated Total Reflectance (ATR) mode on powdered glasses with the grain size 300–500 μm. All IR spectra were recorded within the range 600–1600 cm^{-1} and were corrected for Fresnel losses and normalized to the absorption band with maximum intensity.

The Raman spectra of the preforms and fibers were recorded between 400 and 1500 cm^{-1} at room temperature with a confocal micro-Raman Renishaw Ramascope (system 100) equipped with a Leica DMLM microscope (50× magnification) and connected to a CCD camera. Spectra were collected at 90°. The excitation wavelength (λ_{exc}) of the laser was 514 nm and the power set to $P_{avg} = 20$ mW. The spectral resolution was 2 cm^{-1}.
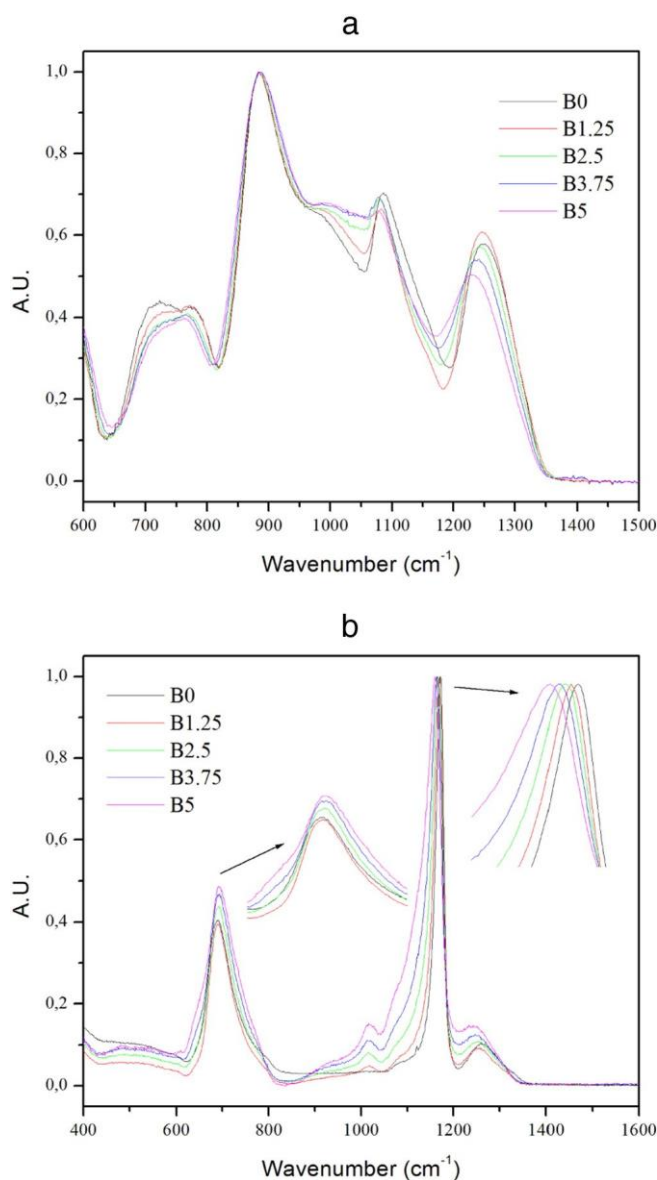
Fig. 1. IR (a) and Raman (b) spectra of the investigated glasses.
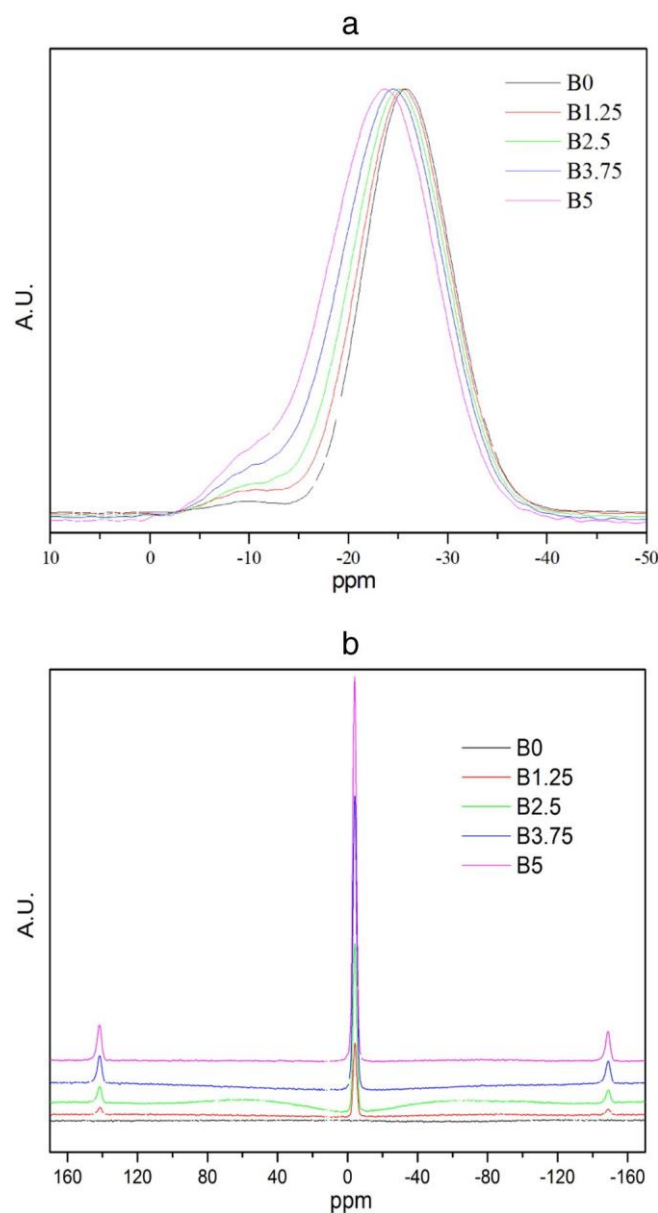
Fig. 2. ^{31}P a) and ^{11}B b) NMR spectra.

Solid State ^{11}B and ^{31}P MAS NMR experiments were carried out with a Bruker Avance 300 spectrometer working at 96 MHz for ^{11}B and 121 MHz for ^{31}P. The spectra were acquired under magic angle spinning (MAS) at a spinning rate of 14 kHz using a 4 mm diameter rotor. A simple pulse sequence was used and the probe signal was subtracted from the spectra acquired to ensure an easier reading. The ^{31}P and ^{11}B chemical shift scales were calibrated with respect to H3PO4 solution and B2O3 solutions, respectively. The spectra were reconstructed thanks to the DMFIT software [16].

Powdered glasses with a grain size of 300–500 μm were immersed in simulated body fluid (SBF) for 336 h at 37 °C in an incubating shaker (Stuart SI500) agitated with an orbital speed of 120 rpm. The SBF was prepared using the protocol developed by Kokubo et al. and following the procedure described in standard ISO/FDIS 23317 [17]. To compare the dissolution kinetics between the glass bulk and the glass fibers, the fibers were cut to a length of 1 cm and the sample mass for both forms was adjusted to give an identical Sa/V ratio. The Sa/V ratio for the powder glass was calculated using the measured density of each glass composition and assuming that the particles were spherical. The changes in the pH of the solutions containing the glass samples and a blank solution were recorded for various immersion times using a

pH/ ion analyzer (Mettler Toledo MA235). Separate samples were studied for each time point. After 24 h, 48 h, 72 h, 168 h and 336 h, the glass powder was filtered, rinsed with acetone and dried. 10 mL of the solution was diluted with 90 mL of ultra-pure water for analyzing the amount of P, Sr, Ca and Na released from the glasses using an Inductively Coupled Plasma–Optical Emission Spectrometer (ICP–OES; Optima 5300DV, Perkin Elmer). The composition of the glass powder and any layers formed at the surfaces during the immersion was studied using SEM/EDXA and ATR as described above. The cutback method was employed to characterize the fiber loss and core absorption spectra, as described by Kaminow and Stulz [18]. A white light source (AQ4305, Yokogawa) was used to inject the light into the fiber on the 600−1700 nm spectral range. The transmitted light was detected by an optical spectrum analyzer (Ando AQ6317B). The initial length of the measured fibers was about 60 cm, and after cutting, the fiber length was reduced to 40 cm. The loss was calculated from the difference of two readings and the length of fiber removed, using the following equation:

$$10\,\frac{Log\left(\dfrac{P_1}{P_2}\right)}{L-l} = dB/m \qquad (2)$$

where P_1 is the output power recorded on a fiber with length L and P_2 the output power recorded on a fiber with length l.

The light transmitted through the fiber was measured in continuous mode using a white light source (Ando AQ4303B) with a wavelength range from 400 to 1800 nm. The light at the fiber output was measured using a light power meter (PM100D from Thorlabs) equipped with a sensor type 150C (λ = 350–1100 nm). The fiber was connected to the light source and the power meter using two bare fiber adapters.
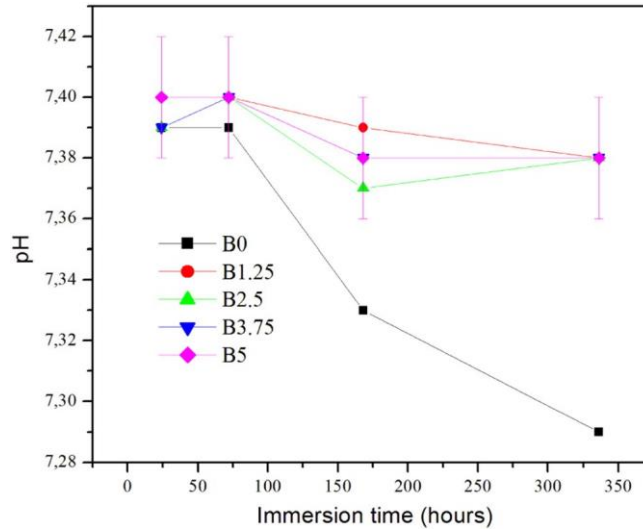

Fig. 3. pH of SBF solution as a function of immersion time.

3. Results and discussion

New phosphate glasses in the system (50 − x)$P_2O_5\cdot$20CaO$\cdot$ 20SrO$\cdot$10$Na_2O\cdot$x B_2O_3 with x = 0, 1.25, 2.5, 3.75 and 5 (mol %) (B0, B1.25, B2.5, B3.75 and B5) were prepared for studying the impact of the replacement of P_2O_5 by B_2O_3 on the thermal, structural and bioactive properties.

The thermal properties as well as the density and the refractive indices of the glasses as a function of the boron oxide content are listed in Table 1. An increase in B_2O_3 induced an increase in the density. Such increase in density is accompanied by a decrease in the molar volume indicating a contraction of the glass network. The glass transition (T_g) and onset of crystallization (T_x) temperatures increased with an increase in the B_2O_3 content thus indicating an increase in the glass network connectivity. The difference between these temperatures, $\Delta T = (T_x - T_g)$, is also listed in Table 1. ΔT provides a gauge of the resistance to crystallization and should be as large as possible for a glass to be drawn into fibers with a good optical quality and minimal scattering loss from microcrystallites [19]. Typically, a ΔT value larger than 100 °C suggests reasonable glass stability. As the preform must sit with- in a heated furnace during drawing, this stability becomes important for successful drawing of a crystallite-free fiber. ΔT is larger than 100 °C for all experimental glasses confirming that the novel borophosphate com- positions developed are suitable glasses for fiber drawing from preform. Additionally, ΔT is the largest for the B2.5 glass suggesting that among the experimental compositions this glass is the most promising candidate for fiber drawing. Similar improvement of the thermal stability was observed with the addition of B_2O_3 in the

P_2O_5–Na_2O glass system [20]. In Table 1 are also listed the refractive indices of the glasses measured at different wavelengths. As expected, the refractive index of the glasses decreased when the wavelength increases.
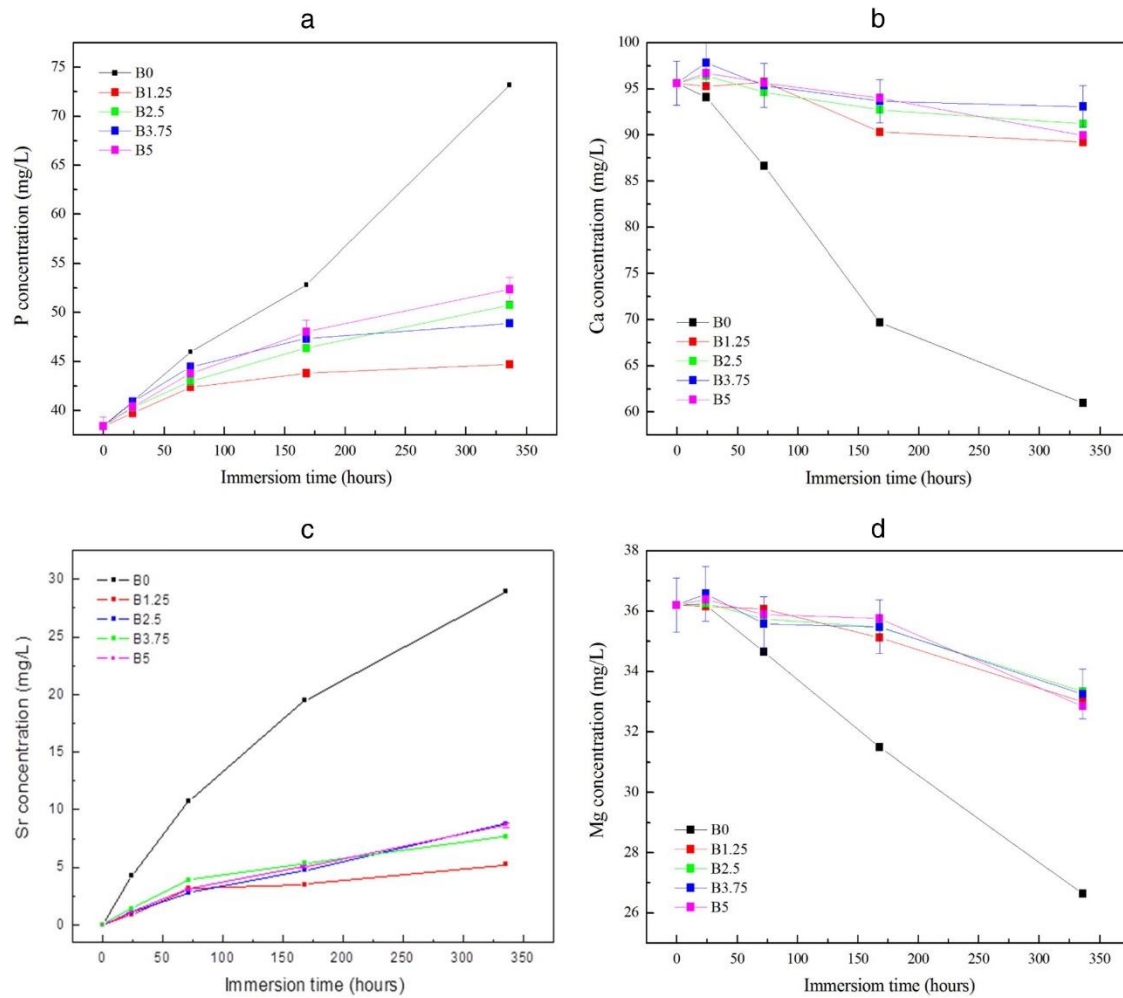
Fig. 4. Average concentration of a) P, b) Ca, c) Sr, and d) Mg in SBF for the boron containing glasses at various immersion times.

Moreover, an increase in the B_2O_3 content increased the refractive index in agreement with the increase in the density. In a core–clad optical fiber used to probe the glass reaction in the body, the core must have a slightly higher B_2O_3 content than the clad to ensure that the light is efficiently transferred to the core of the fiber [21].

The structural properties of the glasses as a function of B_2O_3 content were investigated using ATR, Raman spectroscopy and NMR.

The IR spectra of the glasses are shown in Fig. 1a. All spectra were normalized to the band located at ~ 880 cm^{-1}. The spectra exhibit five absorption bands located around 1260, 1085, 880, 775 and 718 cm^{-1} and two shoulders at ~ 1154 and 980 cm^{-1}. As explained in [20], the region between 1150 and 1400 cm^{-1} is characteristic of vibration of non-bridging PO_2 groups. The band at 1260 cm^{-1} can be assigned to asymmetric stretching modes, $v_{as}(PO_2)$, of the two non-bridging oxy- gen atoms bonded to a phosphorus atom in a Q^2 phosphate tetrahedron. The shoulder at 1154 cm^{-1} corresponds to symmetric vibration of PO^{2-} in Q^2 units. The region in the 900–1150 cm^{-1} range is characteristic of terminal P–O and PO_3 groups. The shoulder centered at ~ 980 cm^{-1} and the band at 1085 cm^{-1} corresponds to the symmetric and asymmetric stretching vibration of PO^{2-} in Q^1 units, respectively [22,23].

The band at 1085 cm^{-1} can be also attributed to an overlap between PO_3 Q^1 terminal group and PO_2 Q^2 groups in metaphosphate [24]. The last region in the 700–900 cm^{-1} domain is characteristic of the vibration of bridging P–O–P groups. The absorption band located at 718 and 775 cm^{-1} is characteristic of P–O–P symmetric stretching vibration in metaphosphate structure [24]. The main band at ~ 880 cm^{-1} is attributed to P–O–P asymmetric stretching of bridging oxygen in Q^2 units (v_{as} P–O–P Q^2) [22,25,26]. The bands at 1085 and 1260 cm^{-1} shifted to- ward lower wavenumbers with increasing B_2O_3 content. Additionally, the increase in the B_2O_3 content leads to a decrease in the intensity of the band at 1085 cm^{-1}, whereas the intensity of the band at 775 cm^{-1} region increased as compared to the main band. It is interesting to point out that the band at 1260 cm^{-1} becomes broader with an increase in the B_2O_3 content. Its intensity increased slightly when the B_2O_3 content increased from 0 to 1.25 and then progressively decreased and also shifted to lower wavenumber when B_2O_3 increased from 1.25 to 5. As explained in [20], no direct information on the interconnection of borate and phosphate units can be obtained because of the overlap of borate and phosphate bands. However, it is possible to relate the increase in the intensity of the band at 770 cm^{-1} to the formation of B–O–B bonds. Also, the shoulder at 980 cm^{-1} can be related to the asymmetric stretching of the $B\emptyset^-$ tetrahedra [27]. The increase in intensity and the shift of the band at 1250 cm^{-1}, when B_2O_3 increases, lead to an increase in BO_4 groups as reported in [10,20,28].

Fig. 1b presents the Raman spectra of the glasses. All spectra were normalized to the band with the maximum intensity peaking at ~1175 cm^{-1}. The spectra exhibit bands at ~ 690, 1010, 1175 and 1250 cm^{-1} and one shoulder at 1095 cm^{-1}. The bands at around 1230 and 1175 cm^{-1} can be ascribed to the asymmetric and symmetric stretching of non-bridging $v(PO_2)$ of Q^2 groups, respectively [29–31]. The band at 1020 cm^{-1} can be related to the stretching $v(P–O)$ of terminal groups (Q^1) and the band at 690 cm^{-1} to the symmetric stretching of bridging $v_s(O–P–O)$ of Q^2 groups [32]. The shoulder at ~ 1095 cm^{-1} corresponds to motion of terminal oxygen bond vibration in phosphate chains [33]. When the B_2O_3 content increased, the bands located at~ 1010, 1175 and 1250 cm^{-1}, along with the shoulder at 1095 cm^{-1} shifted to lower wavenumber whereas the band at 690 cm^{-1} shifted to higher wavenumber. The shift of the main band at 1171 cm^{-1} suggests a weakening of the P–O–P bonds in Q^2 units with an increase in the B_2O_3 content, while the increase in intensity and the low frequency shift of the band at 1255 cm^{-1} can be attributed either to the stretching vibration of B–O bonds in borate triangles [32] or, most probably, to the re-orientation of the Q^2 units in the phosphate network. An increase in the B_2O_3 content leads also to an increase in the intensity of the bands at 690 1010 and 1250 cm^{-1} and also of the shoulder at 1095 cm^{-1} as compared to the main band. The bands at 690 and at 1250 cm^{-1} also became broader for glasses with increasing B_2O_3 content. The broadening of the IR bands in the 850–1200 cm^{-1} region (Fig. 1a) and the Raman band at 690 cm^{-1} can be ascribed to vibration of P–O–B bridges in Q^2 phosphate units as suggested in [34]. This is in agreement with the in- crease in T_g of the glass with an increase in the B_2O_3 content, as seen in Table 1. The increase in T_g indicates an increase in the glass network connectivity. This increase cannot be due to the increase of the P–O–P bonds as the number of these bonds decreased with increasing B_2O_3 content in the glass. Therefore, it is likely that the formation of P–O–B links instead of P–O–P bonds leads to the observed increase in T_g [20]. Similar results were reported in the $P_2O_5–B_2O_3–Na_2O$ glass system [20]. The shoulder

at 960 cm^{-1} in the spectra of the B$_2$O$_3$-containing glasses can be related directly to the presence of BØ$^-$ units in the glass network [35]. The shoulder at 1090 cm^{-1}, which grows in intensity with increasing B$_2$O$_3$, can be associated with the creation of polyphosphate units containing boron atoms (BØ$_3$, BØ$_2$O$^-$ or BØ$^-$) inducing an increasing number of terminal oxygen bonds in the glass network [10]. As a result, the low frequency shift of the band at around 1171 cm^{-1} was observed with increasing B$_2$O$_3$ in the glass. In agreement with [36], the bands in the 1050–1150 cm^{-1} range could be related to the symmetric stretching vibration of the PO^{3-} tetrahedron surrounded by B^{3+} ions (PO$_4$–BO$_4$ groups).
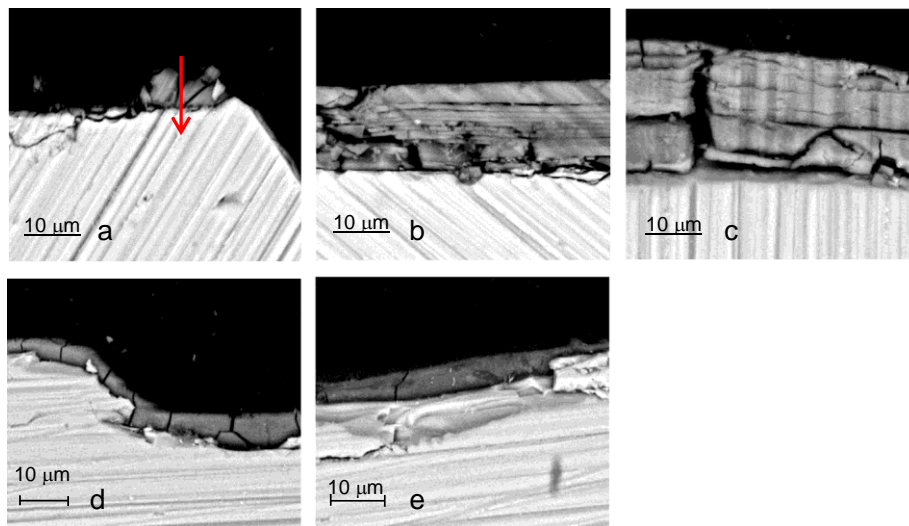

Fig. 5. SEM micrographs of particles of a) B0 at 24 h, b) B0 at 336 h, c) B1.25, d) B2.5 and e) B3.75 glass in SBF at 336 h.

To further support the ATR and Raman analyses, ^{31}P and ^{11}B NMR spectra were recorded. Fig. 2a and b presents the obtained signal of the ^{31}P and ^{11}B spectra for all investigated glasses, respectively. The ^{31}P spectra of the investigated glasses exhibit one major band at −25.7 ppm with a shoulder at −10.5 ppm. The main peak can be attributed to the Q^2 units of the phosphate network, whereas the shoulder can be attributed to Q^1 units [37]. When the B$_2$O$_3$ content increased, the main band shifted to − 23.7 ppm. Deconvolution of the band shows an increase in the Q^1 from 2% to 10% when the boron oxide con- tent in the glasses increases from 0 to 5 mol%. This is in agreement with the analyses of the FTIR and Raman spectra. This can be attributed to the change in the O/P ratio which increases from 3 for x = 0 to 3.22 for x = 5. Clearly, an increase of this ratio led to de-reticulation of the phosphate network and to the emergence of Q^1 species. Such changes can also be attributed to the formation of P–O–B bonds (into or at the end of the chains) due to the presence of BO$_4$ (see below) polyhedra in the network.

Table 2

Thickness of the layer forming at the surface of the investigated glasses at different immersion times.

	Layer thickness (± 3 µm) after immersion h			
	24 h	72 h	168 h	336 h
B0	6	9	12	18
B1.25	0	0	0	21
B2.5	0	0	0	3
B3.75	0	0	0	4
B5	0	0	0	3

When adding B_2O_3, a peak at −3.9 ppm appears and increases in in- tensity, in the ^{11}B NMR spectra, when the concentration of B_2O_3 in- creased (c.f. Fig. 2b). Note that the spectra have been calibrated and are thus quantitative. The narrow line seen in the figure is typical for BO_4 groups [38]. As assumed from the analyses of the FTIR and Raman spectra the amount of BO_4 units increased with the B_2O_3 content. From the ^{11}B NMR spectra no BO_3 units could be detected. Indeed, if present, the BO_3 signal should appear in the 5–15 ppm region [39].

In summary, based on the analysis of the FTIR, Raman and NMR spectra of the glass with x = 0 (B0), the structure was mainly formed of chains of phosphate tetrahedra connected through bridging oxygen with two other phosphate tetrahedra; the out-of-chain oxygen forms terminal PO groups. Thus, the BO_4 units become a part of the structure when B_2O_3 was added. A small addition of B_2O_3 at the expense of P_2O_5 (x from 0 to 1.25) leads first to a decrease in the P–O–P bonds since P–O–B bonds formed and low content of BO_4 units. When added in larger concentration (x N 1.25), the Q^2 units of the phosphate network decreased at the expense of the Q^1 units due to the increasing formation of BO_4 units.

Particles of the size range 300–500 µm of each investigated compositions were immersed in SBF for 24 h, 48 h, 72 h, 168 h and 336 h at 37 °C in an incubating shaker with orbital speed 120 rpm. The pH of the solution was measured for each immersion time. Fig. 3 presents the changes in the pH of the immersion solution as a function of immersion time for various B_2O_3 contents in the glass. The pH of the solution decreased with increasing immersion time for all investigated samples. The decrease was more pronounced for the glass without boron (B0). As the change in the solution pH can be related to the glass dissolution rate [40], the glass B0 was expected to have a higher dissolution rate than the B_2O_3-containing glasses. Based on our former work [41] and also on [42], the dissolution rate of a glass depends on its network dimensionality. The dissolution rate decreases with increasing cross-linking of the glass network. As explained in the previous paragraph, we think that the formation of the P–O–B linkages increases the glass connectivity and thus reduces the glass dissolution rate. The addition of B_2O_3 from 1.25 to 5 did not show any significant impact on the solution pH thus indicating that the increase in the B_2O_3 content up to 5 mol% only slightly impacted the dissolution rate of the glass.

It is well known that the change in the pH is related to the release of ions from the glass into the solution or to the consumption of ions from the solution due to precipitation. Therefore, the concentrations of P, Ca, Sr and Mg ions present in the SBF solution were measured. Note that the Na and B contents could not be quantified as the high sodium content in the SBF led to saturation of the detector and the B content in the solution was below the detection limit. Fig. 4a–d shows the evolution of the concentrations of P, Ca, Sr and Mg in the SBF as a function of immersion time for various boron contents in the glass.

For all the glasses, the P and Sr ion contents in the SBF increased whereas the Ca and Mg ion content decreased with the duration of the immersion. This indicates that the decrease in the pH seen in Fig. 3 can be related to the increase in the content of ions containing P (HPO_4 and PO_4^{3-}) and to the reduction in the content of Ca ions in SBF. The release of the highest concentration of P-containing ions and the consumption of the Ca ions lead to a dramatic decrease in the pH of the solution, as seen in Fig. 3 for the glass B0.

While the glass B0 exhibited the highest increase in the concentration of P and Sr ions in the solution, the glass B1.25 presented the lowest amount of P and Sr ions after 2 weeks of immersion. The solutions containing the glasses with higher B_2O_3 contents (x N 1.25) showed similar release of P and Sr within the accuracy of the measurement. The lower release of P and Sr of the glass B1.25 as compared to the other B_2O_3- containing glasses may be related to the glass structure. As suggested by Vogel et al., the depolymerization of the phosphate chain structure from Q^2 to Q^1 species reduces the

dissolution rate as the Q^2 structure is more susceptible to hydration and subsequent hydrolysis compared to the Q^1 units [43]. Therefore, we think that the formation of P–O–B bonds decreased the dissolution rate when x increased from 0 to 1.25 mol%. The increase in the BO_4 units increased the glass dissolution rate when x increased from 1.25 to 5 mol%. Similar results have been obtained in silicate glasses containing various concentrations of B_2O_3 [44].

As shown in Fig. 4b and d, the concentration of Ca and Mg ions in the SBF containing the glass B0 decreased progressively when the immersion duration increased, whereas the concentration of the same elements decreased only slightly with increasing immersion time for the B_2O_3-containing glasses. No significant differences in Ca and Mg uptake could be seen as a function of B_2O_3 contents in the glass. It is important to remind that a decrease in the Ca and Mg content in the solution indicates that these ions are consumed, i.e. precipitated when the glasses are immersed in SBF. The consumption of Ca from the solution indicates that a reaction layer forms at the surface of the glass when immersed in SBF as reported in [7].
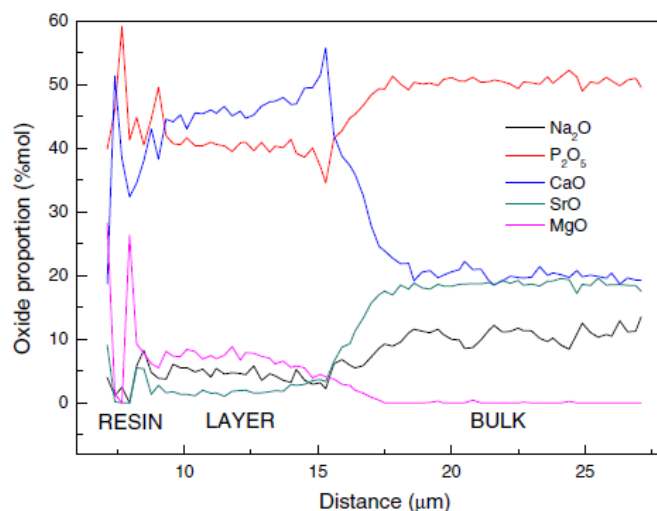

Fig. 6. Composition (mol% oxides) of the bulk glass and surface layer of B0 after 24 h in SBF.

Table 3

The (Ca+Sr+Mg)/P ratio in the reaction layer at the surfaces of the investigated glasses.

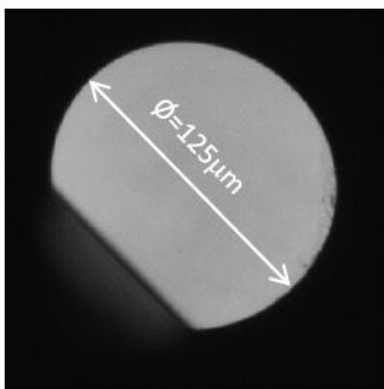|	Duration of immersion in SBF	Composition of the layer (mol%) (±1.5 mol%)					Ratio (Ca + Sr + Mg)/P
		Na_2O	P_2O_5	CaO	SrO	MgO	
B0	24 h	5	40	46	2	7	0.68
B0	336 h	2	35	47	8	8	0.89
B1.25	336 h	2	35	48	8	7	0.91
B2.5	336 h	2	35	51	3	9	0.92
B3.75	336 h	4	34	50	4	9	0.92
B5	336 h	3	35	50	3	10	0.90

Fig. 7. Optical micrograph of the fiber B2.5, 20× magnification.

After 24 and 336 h of immersion, the glass particles were dried, embedded in resin and then polished to examine their cross section using SEM/EDXA. Fig. 5a–e presents the SEM images of glass particles. Fig. 5a and b shows clear signs of a reaction layer at the surface of the particles of glass B0, as expected from our previous data [12]. However, at 24 h of immersion, all B_2O_3 containing glasses did not exhibit any sign of a reaction layer at their surfaces. The first signs of a reaction layer were seen after 2 weeks of immersions (Fig. 5c–e). Table 2 reports the thickness of the reaction layers as a function of immersion time. For the B0 glass, the thickness increased from ~ 6 μm after 24 h to 18 μm after 336 h weeks of immersion in SBF. At 336 h of immersion, the thickness of the layer formed at the surface of the glass B1.75 was similar to the one at the surface of B0, whereas the layer was thinner in the glasses with x N 1.75 indicating that the presence of B_2O_3 in the glass may inhibit the layer formation. We think that the presence of the BO_4 units and maybe of the P–O–B bonds limits the formation of the layer at the surface of the glasses.

The composition of the layer and the bulk glass was estimated using SEM/EDXA. Fig. 6 exhibits the glass/layer composition (mol%) for B0 along the arrow shown in Fig. 5a. The bulk glass composition did not change during the immersion, even after 336 h. The same was observed for all the investigated glasses indicating that the dissolution mechanism of the investigated glasses is congruent. The layer at the surface of the glass B0 contained a lower concentration of Na_2O, P_2O_5 and SrO but a higher concentration of CaO than the parent glass. MgO was also found in the surface layer as suspected from the decrease in the Mg concentration in the solution upon immersion (Fig. 4d). Table 3 summarizes the compositions of the layers at the surfaces of all the investigated glasses. In addition, the (Ca + Sr + Mg)/P ratios are indicated. The concentration of P_2O_5 in the layer at the glass B0 decreased whereas the concentrations of SrO and MgO increase when the immersion increased from 24 to 336 h. The (Ca + Sr + Mg)/P ratio increased from 0.68 to 0.89 with an increase in the immersion time. After 2 weeks in SBF, the layers at the surface of all the investigated glasses had similar (Ca + Sr + Mg)/P ratios of ~ 0.9. This ratio is closer to the (Ca + Sr + Mg)/P ratio for dicalcium phosphate dihydrate [$CaHPO_4 \cdot 2H_2O$, DCPD] than for octacalcium phosphate [$Ca_8(HPO_4)_2(PO_4)_4 \cdot 5H_2O$, OCP], tricalcium phosphate [$Ca_3(PO_4)_2$, TCP] or hydroxyapatite [$Ca_{10}(PO_4)_6(OH)_2$, HAP] [12]. While B_2O_3 delayed the formation of the calcium phosphate layer, this surface layer had similar composition at all investigated glasses.

The preforms with the length of 7 to 10 cm and diameter around 10 mm of the composition B2.5 were drawn into uncoated fiber. Fig. 7 illustrates an optical micrograph of the cross-section of the uncoated fiber. The diameter of the fiber was 125 ± 5 μm. The fiber was circular and concentric. Multiple fibers were examined in a similar manner and no significant variation in the fiber diameter and shape during the drawing process was observed when using the same drawing parameters. The compositions of the resulting fiber were analyzed using EDS. Within the accuracy of the measurement (±1.5 mol%), the fiber composition was identical with the preform. The X-ray diffraction (XRD) patterns of the fibers, not shown here, exhibited only peaks which were attributed to the sample holder. Except those peaks, there was no evidence of crystallization. However, we cannot exclude the presence of crystallites in low quantity and/or a second phase in the fibers.

The propagation losses between 850 and 1450 nm were measured using the cutback method. The homogeneity of the propagation losses along the preforms was checked by 3 to 4 parallel measurements of different pieces of the fiber. One loss spectrum is shown in Fig. 8. Some variations in the propagation loss were observed between the sample fibers ranging from (16 ± 1) to (34 ± 1) dB/m at 1300 nm. These high losses are most probably due to a composition inhomogeneity along the preforms and to a notable quantity of surface or volume defects such as impurities, micro-cracks and bubbles within the glass.
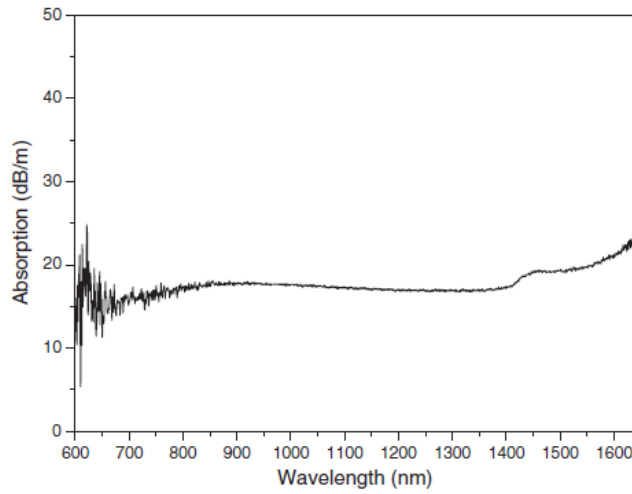
Fig. 8. Loss spectrum of one typical B2.5 fiber.

Micro-Raman spectroscopy was used to evaluate the impact of the fiber drawing on the glass structure. Fig. 9 presents the Raman spectra of the glass prior to and after the drawing. All spectra were normalized to the band with the maximum intensity peaking at ~ 1175 cm^{-1}. The results suggested that the drawing process led to a shift of the main band at 1175 cm^{-1} to a lower wavenumber, and to a small increase in intensity of the band at ~ 1020 cm^{-1} and of the shoulder at 1095 cm^{-1}. These changes indicate that the drawing process leads to a weakening and probable re-orientation of the P–O–P bonds as seen in [21].
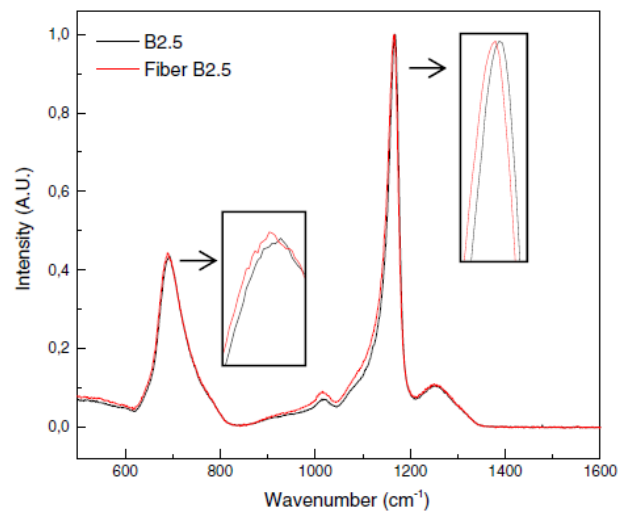
Fig. 9. Raman spectra of the B2.5 preform and the fiber.
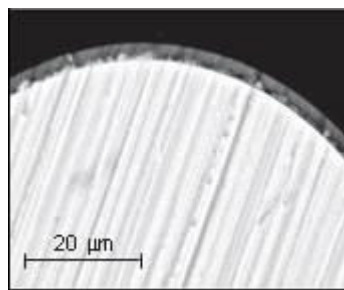
Fig. 10. SEM micrographs of the B2.5 fibers after 336 h in SBF.

Similarly to the bulk samples, also pieces of fibers were immersed in SBF for several weeks at 37 °C in the incubating shaker. No noticeable impact of the fiber drawing process was observed on the decrease of the solution pH and on the release of ions into the SBF. This indicates that the small structural changes induced by the fiber drawing process seen in Fig. 9 had no noticeable impact on the glass dissolution rate. Fig. 10 presents SEM images of chopped fibers after immersion for various time points in SBF. Similarly to the glass particles, the chopped fibers showed a reaction layer at their surface after 336 h in SBF. For glass B2.5, this layer had a similar thickness (~ 4 μm) and also the same composition to the layer at the surface of the particles. No change in the fiber glass composition was found indicating that the dissolution mechanism of the fiber was also congruent similarly to the glass particles.
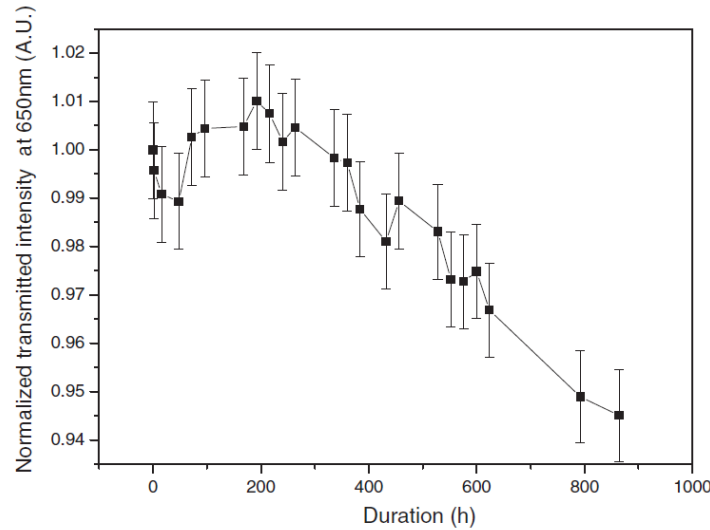
Fig.11. Normalized transmitted light at the output of the B2.5 fiber as a function of immersion duration (hours) in SBF.

Fiber with the total length of 1 m was connected to a light source in one end and to a light power meter at the other end. In the midway, a 7 cm section of the fiber was immersed in 25 mL of static SBF (Sa/V = 0.0053 cm^2/mL) at room temperature and the light output power was collected as a function of immersion time. The normalized light transmitted is given in Fig. 11 as a function of immersion time (h). No change in the transmitted light intensity was observed until ~ 400 h in the solution. After 400 h in SBF, the transmitted light started to slightly decrease. As explained in [21], this reduction in transmitted light intensity as a function of immersion time in SBF can be related to the formation of the Ca–P layer at the fiber surface. Compared to our previous study [21] the decrease of the transmitted light intensity as a function of immersion time in SBF was slower for the fiber with the composition B2.5 than for fiber with the composition $50P_2O_5 \cdot 40CaO \cdot 10Na_2O$ (in mol%). In this work, the transmission in the borophosphate fiber was reduced only by ~ 5% after ~ 800 h in SBF, whereas the transmission was reduced by 94% after 700 h in SBF for the phosphate fiber [21]. This low and slow change in the intensity of the light transmitted through the fiber immersed in SBF is not only due to the addition of B_2O_3 at the expense of P_2O_5 which reduces the dissolution rate of the glass as discussed above but also to the presence of SrO in the glass network. In our previous work [12], we showed that the addition of SrO at the expense of CaO limits the dissolution of the glass and thus decreases the change in the pH of the solution. This study confirms that it is possible to tailor the bioresponse of the bioactive fiber by modifying slightly the composition of the fiber.

4. Conclusions

The effect of P_2O_5 replacement by B_2O_3 on the thermal, structural and bioactive properties of new borophosphate glasses was examined. With increasing substitution of B_2O_3 for P_2O_5, the glass transition and crystallization temperature increased indicating an increase in the glass network connectivity. All studied glasses possessed a ΔT greater than 100 °C indicating that they possessed sufficient resistance to crystallization for shaping the glass into fibers from preforms.

The influence of B_2O_3 content on the glass dissolution was studied in SBF. A layer of calcium phosphate precipitated at all investigated glasses. The thickness of the layer increased with immersion time for the B_2O_3- free glass. After 336 h of immersion, the layer at all glasses showed similar (Ca + Sr + Mg)/P ratio. While the addition of B_2O_3 aimed to obtain a reaction layer with a Ca/P ratio closer to 1.67 the ratio remained at around 0.9. This indicates that replacing B_2O_5 for P_2O_5 up to 10 mol% does not favor precipitation of hydroxyapatite but maintains precipitation of dicalcium phosphate dihydrate which was proven in the past to support cell attachment and proliferation. Small amounts of B_2O_3 (1.25 mol%) reduced the glass dissolution rate probably due to the formation of P–O–B bonds at the expense of P–O–P bonds. Accordingly, the formation of the reaction layer was only slightly delayed. However, for glasses with 1.25 to 5% B_2O_3, the dissolution rate slightly increased. Simultaneously, the rate for layer formation significantly reduced, most probably due to the increase in

the BO$_4$ units in the glass network.

Fibers were successfully drawn from preforms with 2.5 mol% B$_2$O$_3$ (B2.5). Whereas slight changes in the glass structure were observed after fiber drawing, the fiber exhibited similar bioresponse when immersed in SBF than the corresponding glass particles: similar decrease in the pH of solution, release of ions into the solution and same rate for CaP layer formation. Finally, we found that the decrease in the light transmitted through the fiber in SBF decreased when a small amount of P$_2$O$_5$ was replaced by B$_2$O$_3$ due to the slow reaction of this glass in SBF. This further demonstrates that the bioresponse of a phosphate glass can be tailored by suitable B$_2$O$_3$ substitutions (b 5 mol%). In addition, the degradation of the fibers can be followed by recording the change in the output light intensity.

Acknowledgments

References

[1]   M. Marcolongo, P. Ducheyne, W.C. Lacourse, J. Biomed. Mater. Res. 37 (1997) 440–448.
[2]   E. Pirhonen, P. Törmälä, J. Mater. Sci. 41 (2006) 2031–2036.
[3]   D.C. Clupper, M.M. Hall, J.E. Gough, L.L. Hench, Transactions of the Society for Biomaterials, Tampa, FL, 2002.
[4]   L.L. Hench, O.H. Andersson, Bioactive glasses, in: June Wilson (Ed.), An Introduction to Bioceramics, 1993.
[5]   O.H. Andersson, K.H. Karlsson, Corrosion of bioactive glass under various in vitro conditions, Advance in Biomaterials No 8, Elsevier, Amsterdam, 1990.
[6]   J. Massera, S. Fagerlund, L. Hupa, M. Hupa, J. Am. Ceram. Soc. 95 (2012) 607–613.
[7]   J. Clement, J.M. Manero, J.A. Planell, J. Mater. Sci. Mater. Med. 10 (1999)   729–732.
[8]   E.A. Abou Neel, D.M. Pickup, S.P. Valappil, R.J. Newport, J.C. Knowles, J. Mater. Chem. 19 (2009)   690–701.
[9]   W. Liang, Y. Tu, H. Zhou, C. Liu, C. Russel, J. Non-Cryst. Solids 357 (2011) 958–962.
[10] A. Saranti, I. Koutselas, M.A. Karakassides, J. Non-Cryst. Solids 352 (2006)   390–398.
[11] N. Sharmin, M.S. Hasan, A.J. Parsons, D. Furniss, C.A. Scotchford, I. Ahmed, C.D. Rudd, Biomed. Res. Int. 2013 (2013) 1–12.
[12] J. Massera, L. Petit, T. Cardinal, J.J. Videau, M. Hupa, L. Hupa, J. Mater. Sci. Mater. Med. 24 (2013)   1407–1416.
[13] J. Isaac, J. Nohra, J. Lao, E. Jallot, J.-M. Nedelec, A. Berdal, J.-M. Sautier, Eur. Cell. Mater. 21 (2011)   130–143.
[14] J. Vaughan, The Physiology of Bone, 3rd edition Clarendon Press, Oxford, 1981.
[15] J. Massera, A. Kokkari, T. Närhi, L. Hupa, SrO substituted CaO bioactive phosphate- and silicate-based glasses: enhancement of gingival fibroblasts proliferation, J. Mater. Sci. Mater. Med. (2015) (submitted for publication).
[16] D. Massiot, F. Fayon, M. Capron, I. King, S. Le Calvé, B. Alonso, J.-O. Durand, B. Bujoli,
       Z. Gan, G. Hoatson, Magn. Reson. Chem. 40 (2002)   70–76.
[17] T. Kokubo, H. Kushitani, S. Sakka, T. Kitsugi, T. Yamamuro, J. Biomed. Mater. Res. 24 (1990)   721–734.
[18] I.P. Kaminow, L.W. Stulz, Appl. Phys. Lett. 33 (1978) 62–65.
[19] A. Soufiane, M. Poulain, J. Non-Cryst. Solids 161 (1993) 206–209.
[20] D. Carta, D. Qiu, P. Guerry, I. Ahmed, E.A.A. Neel, J.C. Knowles, M.E. Smith, R.J. Newport, J. Non-Cryst. Solids 354 (2008)   3671–3677.
[21] J. Massera, I. Ahmed, L. Petit, V. Aallos, L. Hupa, Mater. Sci. Eng. C 37 (2014) 251–257.
[22] H. GaO, T. Tan, D. Wang, J. Control. Release 96 (2004) 21–28.
[23] E.A. Abou Neel, W. Chrzanowski, D.M. Pickup, L.A. O'Deel, N.J. Mordan, R.J. Newport,
       M.E. Smith, J.C. Knowles, J. R. Soc. Interface 6 (2009) 435–446.
[24] D. Ilieva, B. Jivov, G. Bogachev, C. Petkov, I. Penkov, Y. Dimitriev, J. Non-Cryst. Solids 283 (2001) 195–202.
[25] P.-Y. Shih, H.-M. Shiu, Mater. Chem. Phys. 106 (2007) 222–226.
[26] Y.M. Moustafa, K. El-Egili, J. Non-Cryst. Solids 240 (1998) 144–153.
[27] Y.D. Yiannopoulos, G.D. Chryssikos, E.I. Kamitsos, Phys. Chem. Glasses 42 (2001) 164–172.
[28] A. Yao, M.N. Rahaman, J. Lin, W. Huang, J. Mater. Sci. 42 (2007)   9730–9735.
[29] S. Lee, A. Obata, T. Kasuga, J. Ceram. Soc. Jpn. 117 (2009)   935–938.
[30] M.A. Karakassides, A. Saranti, I. Koutselas, J. Non-Cryst. Solids 347 (2004) 69–79.
[31] A.G. Kalampounias, J. Phys. Chem. 73 (2012) 148–153.
[32] I. Konidakis, C.-P.E. Varsamis, E.I. Kamitsos, D. Möncke, D. Ehrt, J. Phys. Chem. 114 (2010)   9125–9138.
[33] R. Ciceo Lucacel, A.O. Hulpus, V. Simon, I. Ardelean, J. Non-Cryst. Solids 355 (2009) 425–429.
[34] L. Koudelka, P. Mosner, M. Zeyer, C. Jäger, J. Non-Cryst. Solids 351 (2005) 1039–1045.
[35] G.D. Chryssikos, M.S. Bitsis, J.A. Kapoutsis, E.I. Kamitsos, J. Non-Cryst. Solids 217 (1997)   278–290.
[36] J. Yifen, C. Xiangsheng, H. Xihuai, J. Non-Cryst. Solids 112 (1989)   147–150.
[37] D.S. Brauer, N. Karpukhina, R.V. Law, R.G. Hill, J. Non-Cryst. Solids 356 (2010) 2626–2653.
[38] M. Zeyer-Düsterer, L. Montagne, G. Palavit, C. Jäger, Solid State Nucl. Magn. Reson. 27 (2005) 50–64.
[39] K. Bourhis, J. Massera, L. Petit, H. Ihalainen, A. Fargues, T. Cardinal, L. Hupa, M. Hupa,
       M. Dussauze, V. Rodriguez, C. Boussard-Plédel, B. Bureau, C. Roiland, M. Ferraris, Mater. Res. Bull. 63 (2015)   41–50.
[40] K. Franks, I. Abrahams, J.C. Knowles, J. Mater. Sci. Mater. Med. 11 (2000)   609–614.
[41] J. Massera, K. Bourhis, L. Petit, T. Cardinal, L. Hupa, M. Hupa, J. Phys. Chem. Solids 74 (2013)   121–127.
[42] B.C. Bunker, G.W. Arnold, J.A. Wilder, J. Non-Cryst. Solids 64 (1984) 291–316.
[43] J. Vogel, P. Wange, S. Knoche, C. Russel, Glas. Sci. Technol. 77 (2004) 82–87.
[44] J. Massera, C. Claireaux, T. Lehtonen, J. Tuominen, L. Hupa, M. Hupa, J. Non-Cryst. Solids   357 (2011) 3623–3630.